Domain structures as optical gratings controlled by electric field in a bent-core nematic

Ming-Ya Xu,[1] Meng-jie Zhou,[1] Ying Xiang,[1,3,4,*] Péter Salamon,[2] Nándor Éber,[2] and Ágnes Buka[2]

[1]*School of Information Engineering, Guangdong University of Technology, Guangzhou 510006, China*
[2]*Institute for Solid State Physics and Optics, Wigner Research Centre for Physics, Hungarian Academy of Sciences, H-1121 Budapest, Konkoly Thege Miklós út 29-33, Hungary*
[3]*Guangdong Provincial Key Laboratory of Functional Soft Condensed Matter, Guangdong University of Technology, Guangzhou 510006, China*
[4]*frank_xiang68@qq.com*
[*]*xiangy@gdut.edu.cn*

Abstract: A regular domain structure consisting of parallel stripes – flexodomains – have been induced by low frequency (subHz) electric voltage in a bent core nematic liquid crystal. The wavelength of the pattern is in the range of 1–10 micrometers and thus can conveniently be observed in a polarizing microscope. It also serves as an optical grating and produces a regular system of laser diffraction spots. The pattern was found to emerge and disappear consecutively in each half period of the driving, with the wavelength of the flexodomains changing periodically as the ac voltage oscillates. Analyzing the polarization characteristics of the diffracted light, the polarization of the first order spot was found perpendicular to that of the incident light, in accordance with a recent theoretical calculation.

©2015 Optical Society of America

OCIS codes: (050.1950) Diffraction gratings; (180.0180) Microscopy; (160.3710) Liquid crystals.

References and links

1. R. B. Meyer, "Piezoelectric effects in liquid crystals," Phys. Rev. Lett. **22**(18), 918–921 (1969).
2. *Flexoelectricity in Liquid Crystals. Theory, Experiments and Applications,* Á. Buka and N. Éber, eds. (Imperial College, 2012).
3. L. K. Vistin, "Electrostructural effect and optical properties of a certain class of liquid crystals and their binary mixtures," Sov. Phys. Crystallogr. **15**(3), 514–515 (1970). <other>Kristallografiya 15(3), 594–595 (1970)</other>
4. Yu. P. Bobylev and S. A. Pikin, "Threshold piezoelectric instability in a liquid crystal," Sov. Phys. JETP **45**(1), 195–198 (1977). <other>Zh. Eksp. Teor. Fiz. 72(1), 369–374 (1977)</other>
5. A. Krekhov, W. Pesch, and A. Buka, "Flexoelectricity and pattern formation in nematic liquid crystals," Phys. Rev. E Stat. Nonlin. Soft Matter Phys. **83**(5), 051706 (2011).
6. M. I. Barnik, L. M. Blinov, A. N. Trufanov, and B. A. Umanski, "Flexo-electric domains in liquid crystals," J. Phys. France **39**(4), 417–422 (1978).
7. H. P. Hinov and L. K. Vistin, "Parallel and cross-like domains due to d.c. and low frequency (< 2 Hz) electric fields in nematic liquid crystal layers with negative dielectric anisotropy," J. Phys. France **40**(3), 269–292 (1979).
8. P. Schiller, G. Pelzl, and D. Demus, "Analytical theory for flexo-electric domains in nematic layer," Cryst. Res. Technol. **25**(1), 111–116 (1990).
9. V. A. Delev, A. P. Krekhov, and L. Kramer, "Crossover between flexoelectric stripe patterns and electroconvection in hybrid aligned nematics," Mol. Cryst. Liq. Cryst. (Phila. Pa.) **366**(1), 849–856 (2001).
10. P. Kumar and K. S. Krishnamurthy, "Gradient flexoelectric switching response in a nematic phenyl benzoate," Liq. Cryst. **34**(2), 257–266 (2007).
11. M. May, W. Schöpf, I. Rehberg, A. Krekhov, and A. Buka, "Transition from longitudinal to transversal patterns in an anisotropic system," Phys. Rev. E Stat. Nonlin. Soft Matter Phys. **78**(4), 046215 (2008).
12. N. Éber, L. O. Palomares, P. Salamon, A. Krekhov, and Á. Buka, "Temporal evolution and alternation of mechanisms of electric-field-induced patterns at ultralow-frequency driving," Phys. Rev. E Stat. Nonlin. Soft Matter Phys. **86**(2), 021702 (2012).
13. P. Salamon, N. Éber, A. Krekhov, and Á. Buka, "Flashing flexodomains and electroconvection rolls in a nematic liquid crystal," Phys. Rev. E Stat. Nonlin. Soft Matter Phys. **87**(3), 032505 (2013).
14. L. Kramer and W. Pesch, "Electrohydrodynamic instabilities in nematic liquid crystals," In *Pattern Formation in Liquid Crystals*, A. Buka and L. Kramer, eds. (Springer, 1996), pp. 221–256.

15. Á. Buka, N. Éber, W. Pesch, and L. Kramer, "Convective patterns in liquid crystals driven by electric field," In *Self-Assembly, Pattern Formation and Growth Phenomena in Nano-Systems. NATO Science Series II, Mathematica, Physics and Chemistry, Vol. 218,* A. A. Golovin and A. A. Nepomnyashchy, eds. (Springer, 2006), pp. 55–82.

16. A. Krekhov, W. Pesch, N. Éber, T. Tóth-Katona, and A. Buka, "Nonstandard electroconvection and flexoelectricity in nematic liquid crystals," Phys. Rev. E Stat. Nonlin. Soft Matter Phys. **77**(2), 021705 (2008).

17. S. Kaur, A. Belaissaoui, J. W. Goodby, V. Görtz, and H. F. Gleeson, "Nonstandard electroconvection in a bent-core oxadiazole material," Phys. Rev. E Stat. Nonlin. Soft Matter Phys. **83**(4), 041704 (2011).

18. S. Kaur, V. P. Panov, C. Greco, A. Ferrarini, V. Görtz, J. W. Goodby, and H. F. Gleeson, "Flexoelectricity in an oxadiazole bent-core nematic liquid crystal," Appl. Phys. Lett. **105**(22), 223505 (2014).

19. Y. Xiang, Y.-K. Liu, Z.-Y. Zhang, H.-J. You, T. Xia, E. Wang, and Z.-D. Cheng, "Observation of the photorefractive effects in bent-core liquid crystals," Opt. Express **21**(3), 3434–3444 (2013).

20. Á. Buka, T. Tóth-Katona, N. Éber, A. Krekhov, and W. Pesch, "Chapter 4: The role of flexoelectricity in pattern formation," In *Flexoelectricity in Liquid Crystals. Theory, Experiments and Applications*, Á. Buka and N. Éber, eds. (Imperial College, 2012).

21. Y. Xiang, Y.-K. Liu, Á. Buka, N. Éber, Z.-Y. Zhang, M.-Y. Xu, and E. Wang, "Electric-field-induced patterns and their temperature dependence in a bent-core liquid crystal," Phys. Rev. E Stat. Nonlin. Soft Matter Phys. **89**(1), 012502 (2014).

22. Y. Xiang, M. J. Zhou, M.-Y. Xu, P. Salamon, N. Éber, and Á. Buka, "Unusual polarity-dependent patterns in a bent-core nematic liquid crystal under low-frequency ac field," Phys. Rev. E Stat. Nonlin. Soft Matter Phys. **91**(4), 042501 (2015).

23. S. Rasenat, G. Hartung, B. L. Winkler, and I. Rehberg, "The shadowgraph method in convection experiments," Exp. Fluids **7**(6), 412–420 (1989).

24. S. Lu and D. Jones, "Light diffraction phenomena in an ac-excited nematic liquid-crystal sample," J. Appl. Phys. **42**(5), 2138–2140 (1971).

25. T. O. Carroll, "Liquid-crystal diffraction grating," J. Appl. Phys. **43**(3), 767–770 (1972).

26. S. Akahoshi, K. Miyakawa, and A. Takase, "A frequency measurement of the oscillatory motion of the Williams domain in the nematic liquid crystal," Jpn. J. Appl. Phys. **15**(9), 1839–1840 (1976).

27. H. Miike, Y. Kuriyama, H. Hashimoto, and Y. Ebina, "Laser light scattering study on the electrohydrodynamic instability of nematic liquid crystal," J. Phys. Soc. Jpn. **53**(10), 3280–3283 (1984).

28. P. L. Papadopoulos, H. M. Zenginoglou, and J. A. Kosmopoulos, "Optical measurement of the director relaxation time in a periodically reoriented nematic liquid crystal," J. Appl. Phys. **86**(6), 3042–3047 (1999).

29. T. John, U. Behn, and R. Stannarius, "Fundamental scaling laws of on-off intermittency in a stochastically driven dissipative pattern-forming system," Phys. Rev. E Stat. Nonlin. Soft Matter Phys. **65**(4 4 Pt 2A), 046229 (2002).

30. T. John, U. Behn, and R. Stannarius, "Laser diffraction by periodic dynamic patterns in anisotropic fluids," Eur. Phys. J. B **35**(2), 267–278 (2003).

31. T. John and R. Stannarius, "Preparation of subharmonic patterns in nematic electroconvection," Phys. Rev. E Stat. Nonlin. Soft Matter Phys. **70**(2), 025202 (2004).

32. N. Éber, S. A. Rozanski, S. Németh, A. Buka, W. Pesch, and L. Kramer, "Decay of spatially periodic patterns in a nematic liquid crystal," Phys. Rev. E Stat. Nonlin. Soft Matter Phys. **70**(6), 061706 (2004).

33. W. Pesch, L. Kramer, N. Éber, and A. Buka, "Role of initial conditions in the decay of spatially periodic patterns in a nematic liquid crystal," Phys. Rev. E Stat. Nonlin. Soft Matter Phys. **73**(6), 061705 (2006).

34. Z. D. Xu, Y. N. He, M. C. Guo, and X. G. Wang, "Alternating current electric-field-induced tunable microstructures and electrohydrodynamic convection properties observed in azo-dye-doped MBBA liquid crystal cells," J. Appl. Phys. **102**(2), 026101 (2007).

35. J. Heuer, T. John, and R. Stannarius, "Time reversal of the excitation wave form in a dissipative pattern-forming system," Phys. Rev. E Stat. Nonlin. Soft Matter Phys. **78**(3), 036218 (2008).

36. P. Salamon, N. Éber, Á. Buka, T. Ostapenko, S. Dölle, and R. Stannarius, "Magnetic control of flexoelectric domains in a nematic fluid," Soft Matter **10**(25), 4487–4497 (2014).

37. J. A. Kosmopoulos and H. M. Zenginoglou, "Geometrical optics approach to the nematic liquid crystal grating: numerical results," Appl. Opt. **26**(9), 1714–1721 (1987).

38. H. M. Zenginoglou and J. A. Kosmopoulos, "Geometrical optics approach to the obliquely illuminated nematic liquid crystal diffraction grating," Appl. Opt. **27**(18), 3898–3901 (1988).

39. H. M. Zenginoglou and J. A. Kosmopoulos, "Geometrical optics approach to the nematic liquid crystal grating: leading term formulas," Appl. Opt. **28**(16), 3516–3519 (1989).

40. H. M. Zenginoglou and J. A. Kosmopoulos, "Linearized wave-optical approach to the grating effect of a periodically distorted nematic liquid crystal layer," J. Opt. Soc. Am. A **14**(3), 669–675 (1997).

41. W. Pesch and A. Krekhov, "Optical analysis of spatially periodic patterns in nematic liquid crystals: diffraction and shadowgraphy," Phys. Rev. E Stat. Nonlin. Soft Matter Phys. **87**(5), 052504 (2013).

1. Introduction

Nematic liquid crystals (NLCs) are anisotropic fluids with inherent orientational ordering, described by the director **n**. As shown by Meyer [1], the symmetry properties of nematics allow for the existence of flexoelectricity [2], which manifests itself in an electric polarization, $\mathbf{P}_{fl} = e_1 \mathbf{n} \operatorname{div} \mathbf{n} - e_3 \mathbf{n} \times \operatorname{curl} \mathbf{n}$, induced by elastic deformations (by director

gradients). Here e_1 and e_3 are phenomenological flexoelectric coefficients belonging to the splay and bend elastic deformations, respectively. In an electric field **E,** the flexoelectric polarization yields a linear, flexoelectric interaction ($-\mathbf{P}_{fl} \mathbf{E}$), in addition to the usually dominating quadratic, dielectric one ($-\frac{1}{2} \varepsilon_a (\mathbf{nE})^2$, where ε_a is the dielectric anisotropy of the material).

The flexoelectric instability, which is observable in a planarly aligned sandwich cell filled with certain nematics when the applied voltage exceeds some threshold value V_c, is an example for an electric field induced deformation solely due to flexoelectricity. This instability called flexoelectric domains (or shortly flexodomains, FDs) manifests itself as spatially periodic array of bright and dark stripes, which run parallel with the initial director alignment; it was first observed by Vistin [3]. The dc voltage induced patterned state is an equilibrium deformation (without any material flow), having a lower free energy than the initial homogeneous state, as the free energy gain due to the flexoelectric interaction may overcome the increments of the elastic and dielectric contributions [4]. Using the one-elastic-constant approximation, it has been shown that flexodomains may emerge only if the parameter combination $|\mu| = (\varepsilon_0 \varepsilon_a K)/(e_1 - e_3)^2 < 1$; then the threshold voltage $V_c(\mu)$ and the critical wave vector $\mathbf{q}_c(\mu)$ of the pattern were calculated. Here K is the one (averaged) elastic modulus. Recently, a more precise theoretical analysis has taken into account the anisotropy of elasticity, and confirmed that FDs may appear only in a finite μ interval whose boundaries depend on the differences between elastic moduli [5].

The restrictions on μ substantially reduce the number of nematics suitable for studying the flexoelectric instability; indeed, only a few compounds have been reported to exhibit FDs [3,6–13]. Flexodomains are best detectable at dc excitation, even though that introduces some uncertainties into the threshold measurement, as the applied voltage partially drops on the orienting layers and on the ionic double layers formed at the electrodes [12]. Using ac excitation, the capacitive coupling may reduce the influence of this internal attenuation; however, calculations predict a strong increase of V_c with the frequency f of the applied voltage [5], which may provide a practical upper frequency limit for observing FDs. In addition, at higher f and/or if the electrical conductivity σ is non-negligible, dissipative effects (like electric currents and flow due to director relaxation or charge separation) may also have an important role, modifying the mechanism of pattern formation as well as the morphology of the resulting patterns. Then the patterns are classified as those of electroconvection (EC) [14,15] rather than FDs. The frequency f_c, where EC takes over from FDs due to its lower threshold voltage, depends strongly on the material parameters and is usually below a few Hz.

Most materials, where an FD to EC transition has been reported so far [11–13], had opposite sign of their dielectric and conductivity anisotropies ($\varepsilon_a < 0$, $\sigma_a > 0$) and therefore, they exhibited standard electroconvection [15]. In these cases a significant change occurs in the direction of the wave vector $\mathbf{q}_c$ at the transition. If, however, the two anisotropies are of the same sign ($\varepsilon_a < 0$, $\sigma_a < 0$), nonstandard electroconvection occurs [15,16], which is also due to flexoelectricity (as FDs), just involving dissipative couplings in addition to the equilibrium ones. In such compounds one may expect a gradual, smooth transition from FDs to nonstandard EC, without a big change in $\mathbf{q}_c$; that can make distinguishing the two pattern types and identifying f_c difficult [17,18].

When the transition frequency f_c accidentally falls into the subHz range, the period time τ = $1/f$ of the driving sinusoidal ac voltage is much longer than the director relaxation time. Therefore, the patterns (whether FDs or EC) can emerge and decay in each half period; the patterns exist only in a short part of the period (flashes). It has recently been shown that compounds with $\varepsilon_a < 0$, $\sigma_a > 0$ may exhibit in this ultra-low f range both FD and standard EC patterns in a certain voltage range as time separated, alternating flashes [11–13].

As both FDs and EC are stripe patterns (though with different wave vectors), they behave as optical gratings controllable by the applied voltages, which opens up the way for optical applications. Studies of FDs as gratings have been, however, so far quite scarce [19].

In the present paper, we intend to provide a deeper insight into the characteristics of flexodomains, as well as into the yet unexplored ultra-low f behavior of nonstandard EC

exhibited by substances with $\varepsilon_a < 0$, $\sigma_a < 0$. The measurements were performed on a recently synthesized bent-core nematic (BCN) compound. Using complementary experimental techniques, polarizing microscopy and laser diffraction, pattern characteristics and their dependence on frequency, applied voltage and time were explored. Moreover, the unexpected polarization characteristics of the light diffracted on the FD pattern were determined.

2. Material and experimental setup

Measurements were performed on the bent-core nematic liquid crystal 2,5-bis (4-(difluoro (4-heptylphenyl) methoxy) phenyl)-1,3,4-oxadiazole (7P-CF$_2$O-ODBP), whose photorefractive properties have been reported recently [20]. It is the shortest member of a BCN homologous series, whose longer members have also been studied [21,22]. The structural formula of the compound is shown in Fig. 1. The phase sequence is:

Crystal – 77 °C – Smectic – 90.3 °C – Nematic – 131.5 °C – Isotropic.
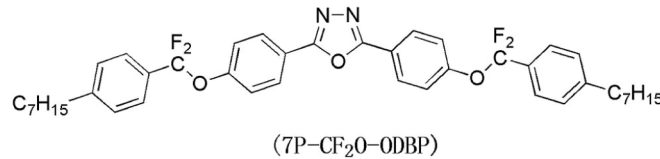

Fig. 1. Structural formula of the BCN compound 2,5-bis (4-(difluoro (4-heptylphenyl) methoxy) phenyl)-1,3,4-oxadiazole (7P-CF$_2$O-ODBP).

Sandwich cells of 6 μm thickness were used. Planar alignment was obtained by a rubbed polyimide layer coated on the indium-tin-oxide transparent electrodes. The cells were filled with the compound in the isotropic phase due to capillary action.

Most experiments were performed using a Leica DM RXP polarizing microscope (POM). The sample was placed into a Linkam LTS 350 microscope hot-stage, whose temperature T was kept within ± 0.01 °C by a TMS 94 temperature controller.

Sinusoidal ac voltage of ultra-low frequency with amplitude of V_p [$V(t) = V_p \sin(2\pi f t)$, $0 < f < 5$ Hz] from a function generator was applied to the sample via a high voltage amplifier. The voltage induced patterns were observed by the shadowgraph technique [23]; the sample was illuminated by unpolarized white light and a single polarizer (the analyzer) was inserted in the light path after the objective in order to enhance the pattern contrast (it cuts out the ordinary component of light which would pass the sample without becoming spatially modulated). Image sequences were recorded by a fast black-and-white camera (Mikrotron EoSens MC 1362) capable of 2000 frames/s recording rate at the spatial resolution of 512*512 pixels. Image recording was synchronized to the zero crossing of the applied voltage.

POM observations were supplemented by complementary diffraction measurements. The voltage induced patterns correspond to an optical grating of spacing Λ, which therefore, diffracts the incoming laser beam ($\lambda = 633$ nm) producing a set of diffraction spots. The diffraction angles ϕ_κ of the κth order are determined by the relation $\Lambda \sin\phi_\kappa = \kappa \lambda$. This far field diffraction image could be recorded by a digital camera. Alternatively, dynamics of the diffracted spots could also be investigated by a set of $n = 9$ photodetectors, placed at fixed angles ϕ_m within the diffraction angle range ϕ_{min}–ϕ_{max}. Here ϕ_{min} and ϕ_{max} are the diffraction angles of the first order diffraction spot at the onset of the pattern and at the highest applied voltage, respectively. Photodetector signals, which are proportional to the intensity I_m of the light diffracted at the angle ϕ_m of the mth detector, were monitored by an oscilloscope.

3. Experimental results and discussion

In the following, we summarize the results obtained by the POM and diffraction techniques, respectively, about the morphologies and dynamics of FDs and EC patterns. As ultra-low

excitation frequencies were used, special attention has been devoted to their time dependence within a single ac period.

3.1 Voltage and frequency dependence of the pattern morphologies observed by POM

The various observations with POM were performed at the fixed temperature of $T - T_c = -20$ °C; here T_c is the clearing point of the nematic.
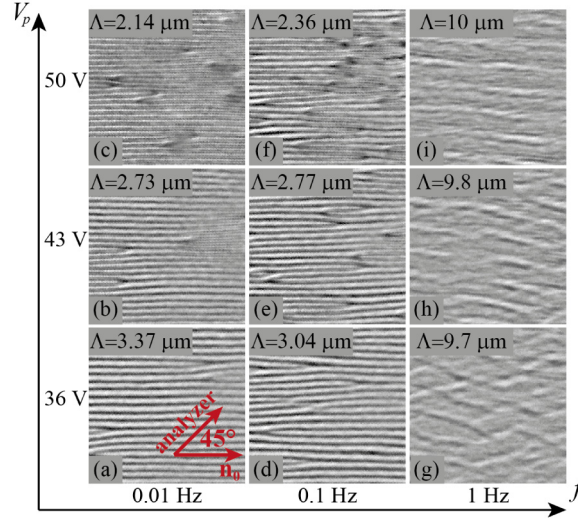
Fig. 2. Variation of pattern morphology with the frequency (f = 0.01 Hz, 0.1 Hz and 1.0 Hz) and the applied voltage (V_p = 36 V, 43 V and 50 V). The arrows indicate the directions of the initial director $\mathbf{n}_0$ and of the analyzer. The size of the POM snapshots is 67 μm × 67 μm.

As an illustration, Fig. 2 exhibits snapshots of the patterns for three frequencies (f = 0.01 Hz, 0.1 Hz and 1 Hz) and three voltage levels (V_p = 36 V, 43 V and 50 V). All snapshots were taken at the maximum of the applied ac voltage, i.e., at the moment of $t = \tau/4$. At the two lower frequencies one finds FDs running parallel with $\mathbf{n}_0$. Their wavelength Λ does not vary much with the frequency, but is very sensitive to the applied voltage level; increasing V_p leads to a substantial decrease of Λ. At f = 1 Hz, however, EC patterns (oblique rolls) appear with a significantly larger wavelength. Increasing the voltage at this frequency causes a change of the obliqueness angle (the stripes become more parallel with $\mathbf{n}_0$) instead of changing the wavelength.

3.2 Temporal variation of the morphologies within a single half period

At ultralow frequency driving, the patterns are not stationary, but emerge and decay within each half period. This is demonstrated in Fig. 3, which shows a sequence of pattern snapshots taken at regular intervals within a single half period at f = 0.1 Hz for FDs [see Figs. 3(a)-3(g)] and at f = 1.0 Hz for EC [see Figs. 3(o)-3(u)]. In addition, Figs. 3(h)-3(n) show the diffraction spots of FDs measured independently at the same frequency, though at higher voltage than that of Figs. 3(a)-3(g). That ensured clearer visibility of the diffraction spots; moreover, it allowed demonstrating the variation of the diffraction angle within the driving period, which will be discussed in more detail in Sec. 3.4.

On the one hand, it is seen that both kinds of patterns exist only in a part of the half period. On the other hand, Fig. 3 clearly demonstrates that the temporal evolution of EC and FDs are completely different. With the time t elapsing, FDs become strongest when $t \to \tau/4$ or $t \to 3\tau/4$, i.e., where the applied voltage and thus the electric field reach their maxima, while they gradually decay as t approaches 0, $\tau/2$ or τ, when the voltage is zero. One can thus say that FDs are roughly in phase of the applied voltage, however, they appear only when the actual voltage exceeds some threshold value. This supports the assumption that in the ultra-

low f range FDs still may be regarded an equilibrium deformation, as dissipative contributions due to director relaxations (e.g. backflow) are negligible; i.e., formation of FDs is driven by the electric field.
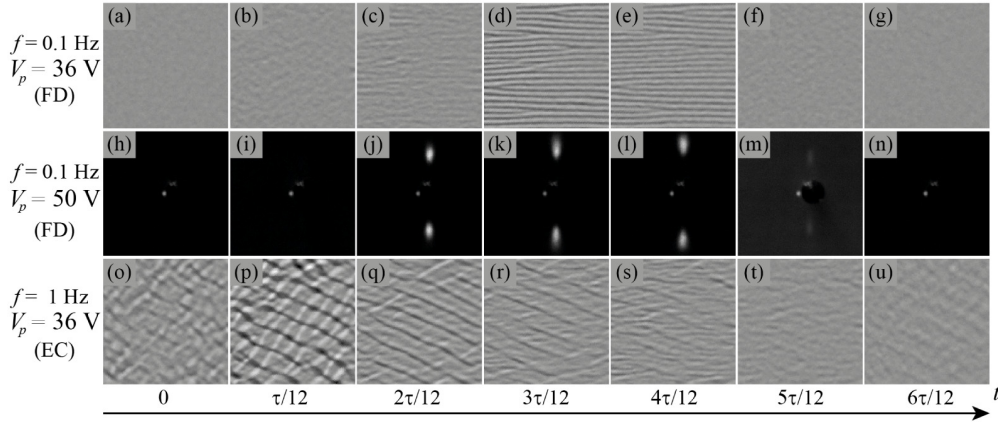

Fig. 3. Morphological changes within a half period. (a)–(g): POM snapshots of flexodomains (FDs) at $f = 0.1$ Hz, $V_p = 36$ V; (h)–(n): snapshots of diffraction spots of FDs at $f = 0.1$ Hz, $V_p = 50$ V (the direct beam is almost completely blocked); (o)–(u): POM snapshots of EC patterns at $f = 1.0$ Hz, $V_p = 36$ V. The size of the POM snapshots is 67 μm × 67 μm.

In contrast to that, one finds that the EC pattern contrast is the highest soon after each polarity-reversal ($t = 0$, $\tau/2$, τ) of the applied voltage and already decays when, at $t \to \tau/4$ or $3\tau/4$, the voltage reaches its maximum. Taking into account that an LC cell corresponds to a mostly capacitive load, the phase of current should be ahead of the voltage by $\pi/2$, which results in maximum currents at $t \to 0$, $\tau/2$, and τ. This correlation between the phase of the current and the onset of EC shows its dissipative behavior and that the EC instability, unlike the FDs, is driven by the current rather than the voltage or field.

3.3 Temporal evolution of the pattern contrast within a driving period

The features, discussed above and illustrated in Fig. 3, can be more precisely explored if one plots the contrast of the pattern versus time. For a satisfactory temporal resolution, a sequence of 2000 images was recorded within a single driving period by the fast camera. The contrast C of the pattern was defined as the mean square deviation of the pixel intensities I_{xy} over the image: $C = \langle (I_{xy} - \langle I_{xy} \rangle)^2 \rangle$. In the homogeneous state, C is nearly zero (its value is determined by the orientational thermal fluctuations of the planar state), but grows with the appearance of the periodic modulation (the pattern). Figure 4(a) shows the time dependence of the contrast at a fixed V_p for the three frequencies, $f = 0.01$ Hz, 0.1 Hz and 1 Hz, together with the instant values of the applied voltage. It is seen that the contrast curves are symmetric; the shape is roughly the same for the positive and negative half cycles. This indicates that the contrast has no polarity dependence. The largest contrast was obtained at the highest frequency ($f = 1.0$ Hz). Here a high, sharp peak is seen in the interval $0 < t < 0.1 \tau$, which transforms into a wide shoulder with a small second peak at $t \approx 0.33 \tau$ before fading to the background for $t > 0.47 \tau$. Reducing the frequency by a decade ($f = 0.1$ Hz), a minor peak is still noticeable at $t \approx 0.03 \tau$, nevertheless the main feature is a wide, flat maximum for $0.12 \tau < t < 0.42 \tau$. At a further decrease by a decade ($f = 0.01$ Hz), only this latter maximum is observable.

Though the contrast, as we defined above, indicates the appearance of patterns, it cannot distinguish the different types, EC and FD. However, based on Fig. 3, it is clear that the narrow peak at $t < 0.1 \tau$ corresponds to EC, while FDs belong to the wide one centered at around t $\approx 0.27 \tau$. Thus the EC and FD patterns occur in different time slots within the half period; at lower f the FDs, at higher f EC dominates. The contrast of FDs follows the applied voltage with only a small phase delay. The change of the heights of the EC peak relative to

that of the FDs indicate that there is a crossover frequency (between 0.1 Hz and 1 Hz), below which FDs are the primary instability, while above that EC has lower threshold voltage.
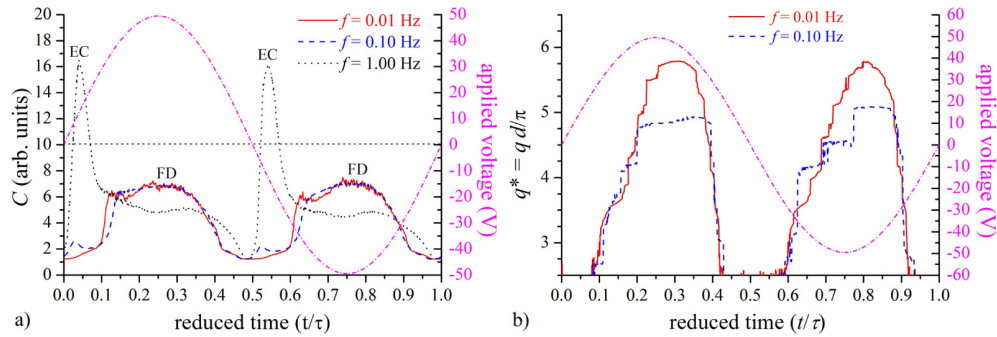

Fig. 4. Temporal evolution of the applied voltage (dash-dotted line) and (a) the pattern contrast C within one period of driving for f = 0.01 Hz, 0.1 Hz and 1.0 Hz at V_p = 50 V; (b) the dimensionless wavenumber $q^*(t/\tau)$ of the FD pattern within a single driving period (τ) for f = 0.01 Hz, V_p = 50 V and for f = 0.1 Hz, V_p = 50 V.

Note that at the two low f cases (f = 0.01 Hz and 0.1 Hz), the steep increase in the FD contrast occurs at about the same reduced time t/τ ($\approx$0.1 and 0.6), i.e., at about the same instantaneous value of the applied voltage; the decay of the contrast follows the same curve.

3.4 Temporal variation of the wavelength within a period

It could clearly be seen in Fig. 2 that the wavelength Λ of FDs are sensitive to the applied voltage. Figure 3 has shown that at the ultra-low f driving the existence of the pattern is closely related to the instantaneous value of the applied ac voltage. As the voltage changes slowly compared to the director relaxation time, it might be expected that the wavelength of the pattern is also changing within the driving period. Indeed, the measurements provided a proof that Λ does not remain constant within the period. This is demonstrated in Fig. 4(b), which exhibits the time dependence of the dimensionless wavenumber $q^* = q\ d/\pi = 2d/\Lambda$. While Fig. 4(a) showed that at both ultralow frequencies FDs appear at about the same instantaneous voltage (at the same t/τ), Fig. 4(b) proves that FDs appear with the same q_c. Just as the contrast, q^* also follows the applied voltage with a small phase delay. The $q^*(t/\tau)$ curves almost coincide, except that the maximal value of q^* slightly increases with the reduction of f. This may be an indication that FDs have a slow dynamics; changing the wavelength of FDs requires a long time (seconds). This is not surprising, as stripe patterns are expected to be able to adjust their wavelength only via defect generation and defect motion.

3.5. Diffraction on the patterns and its dynamics

Light diffraction is a complementary method to polarizing microscopy for characterizing patterns. Though the method can easily detect the emergence of patterns and is suitable to provide information about the morphology (the wave vector) and dynamics (temporal evolution of diffracted intensity), in the rare cases when it was used for quantitative characterization, it was applied mostly for EC patterns [24–35]. Here we report on using the diffraction technique to explore the dynamics of FDs. In addition, we also studied the polarization of the diffracted light.

A straightforward way to investigate the diffraction on FDs is to use the fast camera, which can record a time sequence of diffraction spots; thus allowing detection of their displacement. As an example, Figs. 3(h)-(n) show such a time sequence of diffraction spots (the 1st order ones), which correspond to the morphologies of Figs. 3(a)-(g), and is repeated for each half period. It is clear to see that the spots are located along the vertical axis; however, their separation and thus the wavelength of FDs undergo a periodic change.
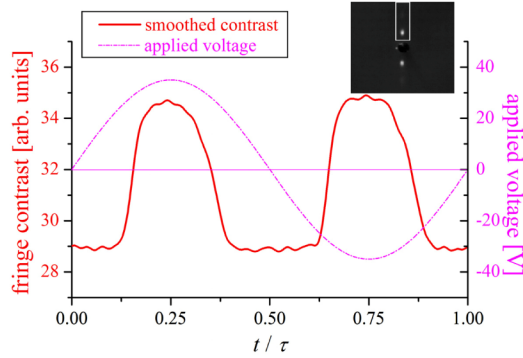
Fig. 5. Smoothed contrast of the diffraction spots (defined as the average intensity of the framed region of the inset picture) vs. time in one driving period at $f = 0.1$ Hz, $V_p = 35$ V. The applied voltage is also shown by dash-dotted line.

Figure 5 shows an example for the temporal evolution of the contrast of the diffraction spots within a single ac period, recorded at $T - T_c = -17$ °C, $f = 0.1$ Hz, $V_p = 35$ V. Here the contrast of the diffraction spots was defined as the average intensity in a wide region along the upper half of the vertical axis (as shown in the inset of Fig. 5). It may include higher than first order spots (if there are any), but excludes contributions from the direct beam (0th order) and its reflections. In order to reduce the noise of the contrast curve, an FFT smoothing algorithm was applied. The contrast of the spots correlates closely with the diffraction efficiency, which becomes strongest at about $t = \tau/4$ or $t = 3\tau/4$, where the electric field is maximum, and decreases to minimum at about $t = 0$ or $t = \tau/2$ where the electric field vanishes. The shape of the contrast plot in Fig. 5 is very similar to the plot (blue dashed line) in Fig. 4(a). This is not surprising because both the contrasts of the pattern and of the spots depend on the amplitude of the flexoelectric deformation of the BCN.

A detailed study of the spot sequences recorded within a period shows that the 1st order spot appears at a diffraction angle $\phi = \phi_{min}$. Upon increasing the voltage, the wavelength of the FDs decreases; hence the diffraction angle grows until it reaches its maximum value $\phi = \phi_{max}$ at about the voltage maximum (after 1/4 period of the driving voltage). After that, the diffraction angle reduces back to ϕ_{min}, where the spot disappears, and the whole process is repeating for the next half cycle.

Besides visualizing the diffraction spots by a digital camera, the oscillating dynamics of the diffracted light was also be monitored by a set of n photoelectric detectors positioned equidistantly to different diffraction angles ϕ_m, between $\phi_1 = \phi_{min}$ and $\phi_n = \phi_{max}$. The corresponding optical set-up is shown in Fig. 6. The signal of the mth photodetector is proportional to the intensity diffracted at the angle ϕ_m. As the wavelength of FDs increase and decrease periodically with the applied voltage, the diffracted light sweeps from ϕ_{min} to ϕ_{max} and then back to ϕ_{min}, passing through the detector positions twice in both directions for $1 \leqq m < n$; thus one finds four pulses in a period (centered around the moments $t_{m1}, t_{m2}, t_{m3}, t_{m4}$ with maximal intensities $I_{m1}, I_{m2}, I_{m3}, I_{m4}$, respectively). For $m = n$ the number of pulses reduces to two. In the following, we report on the relations between the parameters ϕ_m, t_{mi}, I_{mi} ($i = 1$–4) and the control parameters V_p and f.
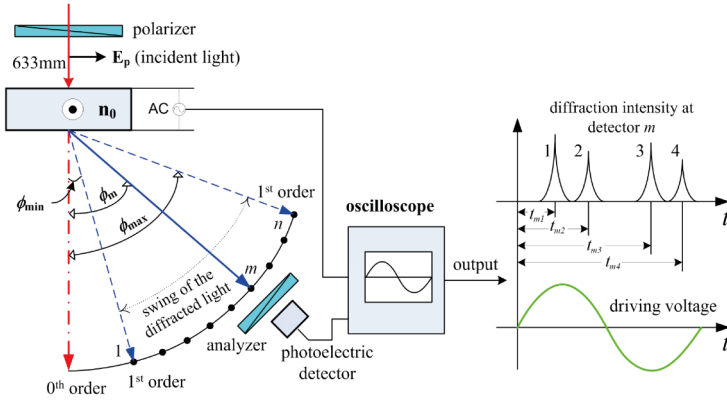
Fig. 6. The set-up for monitoring the dynamics of the diffracted light, and an example of the time dependent intensity signal from the mth detector.
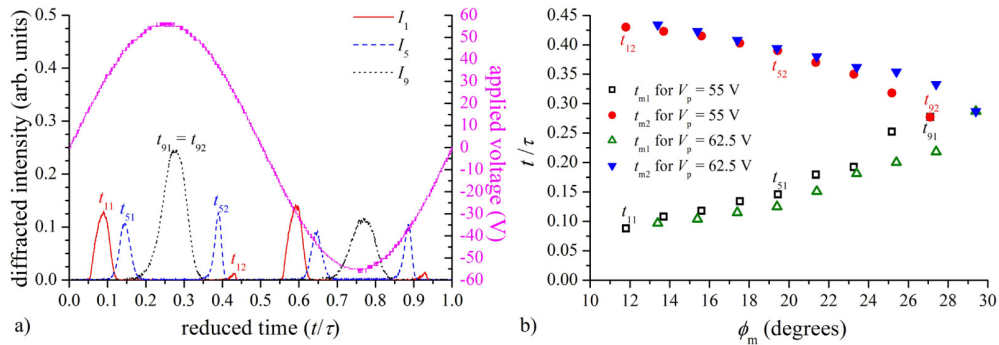

Fig. 7. (a) Temporal evolution of the applied voltage and the 1st order diffraction intensity I_m at selected detector positions ($m = 1, 5, 9$) for f = 0.01 Hz, V_p = 55 V. As the wavelength varies within a driving period, the diffracted light passes these detector positions at different moments and with different intensity. (b) Dependence of the moment (t/τ) of the pulse center on the diffraction angle ϕ_m (the position of the mth detector) within one half period at f = 0.01 Hz for two different V_p.

3.6 Temporal variation of the diffracted intensities within one period

Figure 7(a) depicts the time dependence of the diffracted intensities at selected diffraction angles ϕ_m ($m = 1, 5$ and 9) for $f = 0.01$ Hz, $V_p = 55$ V, i.e., well above the threshold. The pulses at the different detector positions occur at different time slots and with different intensities. The time separation between the two pulses of the same half period is the largest for $m = 1$, and reduces with increasing m. For the last detector $m = n$ ($= 9$ in this case), the two pulses merge into one, indicating the position of the maximal diffraction angle. This behavior is confirmed in Fig. 7(b), which shows the time instants of the center of the detector peaks as a function of the diffraction angle. It is seen that both t_{m1} and t_{m2} converge to a common value ($t/\tau \approx 0.27$) at $m \rightarrow n$. The maximal diffraction angle increases with V_p indicating a shorter wavelength, as expected; however, ϕ_{min} does so too, i.e., the diffraction angle and thus Λ at the pattern onset also depends on V_p. The diffraction efficiency (the intensity I_m) was found to depend on V_p and on the diffraction angle ϕ_m in a non-monotonic way.
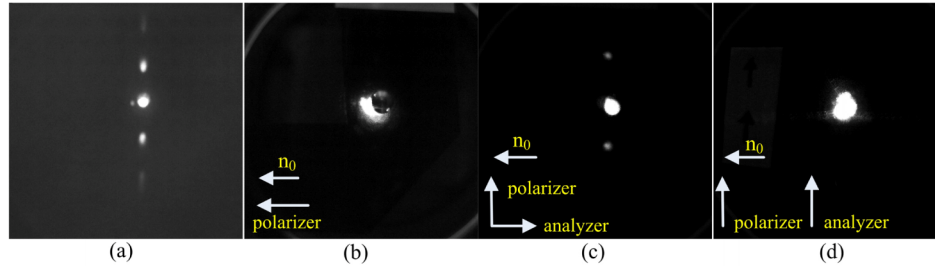
Fig. 8. Visibility of the diffraction spots at different polarizer/analyzer settings: (a) without any polarizer (**P**) or analyzer (**A**); (b) with a single polarizer at (**P**) ∥ $\mathbf{n}_0$; (c) with crossed polarizers at (**P**) ⊥ $\mathbf{n}_0$ and (**A**) ∥ $\mathbf{n}_0$; (d) at parallel polarizer and analyzer at (**P**) ⊥ $\mathbf{n}_0$ and (**A**) ⊥ $\mathbf{n}_0$.

3.7 Polarization characteristics of the diffraction spots

In the diffraction set-up in Fig. 6, the sample was illuminated by an unpolarized laser beam at normal incidence. The polarization characteristics of the incoming beam could be controlled by inserting a polarizer into the light path before the sample; the diffracted beam could be analyzed by inserting and rotating an analyzer after the sample. The results obtained on the polarization characteristics are summarized as follows:

    I. If neither a polarizer, nor an analyzer is inserted, the 1st order diffraction spots are clearly visible, as shown in Fig. 8(a);

    II. Inserting a polarizer P along the initial BCN orientation $\mathbf{n}_0$ (**P** ∥ $\mathbf{n}_0$), the 1st order diffraction spots disappear, as shown in Fig. 8(b);

    III. If we rotate the polarizer out of the **P** ∥ $\mathbf{n}_0$ position towards **P** ⊥ $\mathbf{n}_0$, the 1st order diffraction spots reappear.

       Keeping the polarizer at **P** ⊥ $\mathbf{n}_0$, an analyzer **A** was inserted in order to check the polarization state of the 1st order spot:

    IV. When **P** ⊥ **A**, the 1st order spot is very bright, as seen in Fig. 8(c);

    V. If, however, **P** ∥ **A**, the 1st order spot vanishes, as seen in Fig. 8(d).

These results demonstrate that after being diffracted by FD, the polarization state of the 1st order spot was perpendicular to that of the incident light, which differs from the behavior of conventional EC rolls where the polarization state of light does not change.

4. Discussion and conclusions

In the present paper, we characterized the patterns of a banana nematic LC, 7P-CF$_2$O-ODBP, induced by very low frequency (f < 3 Hz) ac voltages; i.e., at frequencies which are much lower than the typical f range of pattern formation studies. Two kinds of patterns, flexodomains and electroconvection, could be identified.

As in the studied frequency range the director relaxation time of the sample is much shorter than the period of the driving voltage, we found (in agreement with our expectations) that both kinds of patterns exhibit a flashing character; they emerge and decay within a half period of the driving voltage. The variation of the pattern contrast within the period, shown in Fig. 4(a), strongly resembles the former observations on calamitic nematics [11–13]: EC occurs following the zero crossing of the applied voltage, while FDs are seen around the voltage maxima/minima. The strong similarity in the position (phase) of the contrast peaks is not at all trivial, as 7P-CF$_2$O-ODBP is assumed to have the dielectric and the conductive anisotropies both negative, thus enabling nonstandard EC as its longer homologues [19,20], while the calamitics mentioned above had ε_a < 0, σ_a > 0 and exhibited standard EC. In [12] the phases of the EC and the FD peaks could be calculated using the extended standard model of

EC [16] for a calamitic (Phase 5) with known material parameters, concluding that if the internal voltage attenuation and phase shift due to the alignment layers are compensated, the measured phase of FDs coincide with the theoretical predictions, while standard EC occurs earlier in the period than expected. The fact that the phase of the FD peak in 7P-CF$_2$O-ODBP is practically the same as in Phase 5 implies that this phase is not too sensitive to small variations of the material parameters (elastic moduli and permittivities). On the other hand, no theoretical predictions for the phase of a nonstandard EC peak are available yet. Nevertheless, the argument that the earlier emergence of standard EC may be triggered by the ionic current peaks following the polarity reversal [13] may hold in the case of nonstandard EC too.

A characteristic feature of FDs, distinguishing them from EC, is their change of the wave number with time within the driving period, as shown in Fig. 4(b). It is well known [6,10,36] that the wave number of dc voltage induced FDs increases linearly with the voltage. On the one hand, a half period of an ultra-low frequency ac voltage may be approximated as a slowly varying dc voltage; therefore the temporal evolution of q may be attributed to the temporal variation of the instantaneous voltage. On the other hand, the fact that the maximal value of q at the same voltage increases as f is reduced, despite of the increasing threshold, indicates that even at the studied very low frequencies the voltage variation is still not slow enough for the system to reach the local equilibrium.

Diffraction measurements revealed another specific feature of FDs: the polarization direction of the first order diffracted light is perpendicular to that of the incident laser beam. Relating the properties (intensity and polarization) of the diffracted light to the periodic director modulation in the nematic layer is a basic problem of diffraction optics. Former theoretical models based on geometrical optics [37–39] or physical optics [30,40] assumed a one-dimensional deformation in the plane normal to the cell, which was a fairly good approximation for EC patterns. They concluded that at normal incidence of light, the incoming and outgoing polarization directions are the same and for standard EC the first order diffracted intensity is negligible compared to the second order one. The assumption of one-dimensional deformation, however, does not hold for the flexodomains, which involve periodic modulation of the tilt angle as well as the azimuthal angle of the director. A recent generalization of the theoretical optical analysis to arbitrary three-dimensional director fields have shown [41] that the diffracted light can have a component with polarization perpendicular to that of the incoming beam in the presence of twist, i.e., a variation of the azimuthal angle along z. This requirement fulfils for FDs; therefore, the detection of first order diffracted spots at crossed polarizers in case of normal incidence is in accordance with the theoretical predictions.

Finally, we would like to emphasize that there is a crossover frequency where the primary instability changes its type due to the intersection of the $V_c(f)$ threshold curves of FDs and EC. As usual, FDs are observable at lower frequencies. In view of possible future applications of the FDs as controllable gratings, thus decreasing their threshold voltage and/or pushing up the EC threshold voltage of materials is an important task.

Acknowledgments